

PACS numbers: 42.62.Eh; 07.60.Ly; 06.30.Ft
DOI: 10.1070/QE2004v034n12ABEH002746

Spectral and temporal characteristics of a supercontinuum in tapered optical fibres

S.N. Bagayev, V.I. Denisov, V.F. Zakhar'yash, V.M. Klement'ev, S.M. Kobtsev, I.I. Korel', S.A. Kuznetsov, S.V. Kukarin, V.S. Pivtsov, S.V. Smirnov, N.V. Fateev

***Abstract*. The emission spectrum of a femtosecond Ti : sapphire laser broadened in a tapered optical fibre and the shape of its envelope are studied as functions of the waist diameter and the laser power coupled to the fibre. By varying the fibre parameters and characteristics of coupled pulses, the envelope of the broadened emission spectrum can be shaped, which is important in using a femtosecond comb for precision measurements. The results of experimental studies of the temporal structure of a supercontinuum in a tapered fibre obtained by using the sum frequency generation are presented for the first time and theoretically interpreted.**

Keywords: *femtosecond laser, optical fibres, nonlinear optics, supercontinuum.*

1. Introduction

One of the important problems of quantum electronics is the development and fabrication of optical frequency standards. It becomes obvious with time that precision metrological measurements are more and more necessary in the optical spectral region, especially for navigation and communication systems, as well as for measurements of physical quantities, in particular, fundamental constants. When a laser frequency standard is used for such precision measurements, it is often necessary to transfer its frequency characteristics to different spectral ranges. Because frequency standards are mainly used in the radio-frequency region, the frequency characteristics of optical standards should be transferred to the radio-frequency region, which requires an optical clock. The latter consists of an optical frequency standard and a system for frequency division from the optical to radio-frequency region. The first frequency-division systems were complex and cumbersome setups consisting of a chain of specially selected and phase-locked lasers emitting in the near-, mid-IR, and submillimetre ranges, microwave oscillators, and fast frequency converters [1]. Frequency converters of a similar design assume the presence of a set of output frequencies.

The idea of using a cw ultrashort-pulse laser in optical frequency standards and in ultrahigh-resolution laser spectroscopy was proposed more that twenty years ago in papers [2 – 4]. This idea was experimentally realised by using a synchronously pumped cw picosecond dye laser [3]. However, a real breakthrough was achieved only recently due to the rapid development of femtosecond lasers [5, 6] and the appearance of special optical fibres used for the laser spectrum broadening (photonic-crystal or holey fibres and tapered fibres) [7 – 12].

A femtosecond laser generates a train of pulses with a period equal to the round-trip transit time for light in the laser resonator. The emission spectrum of such a laser is a comb of equidistant frequencies (modes). By stabilising this femtosecond comb with the help of a frequency standard, we obtain a set of stable optical and intermode frequencies which are located in the radio-frequency range. There exist several schemes of employing the femtosecond comb for precision measurements of absolute optical frequencies and frequency intervals in the optical region. Any frequency lying within the interval covered by the frequency comb can be determined by measuring simply the beat frequency between this frequency and the nearest mode of the comb.

The use of the femtosecond comb in metrology is simplified when the width of the comb spectrum covers an octave, i.e., when the maximum frequency in the comb is twice as large as the minimum frequency. However, even for the shortest pulse (a 5-fs pulse from a Ti : sapphire laser at 0.8 μm), such a broad spectrum is not achieved. Therefore, the problem appears of increasing the width of the comb spectrum by preserving a strictly equidistant location of frequencies. This problem is often solved by using photonic-crystal or holey fibres and tapered fibres, which allow the generation of a supercontinuum (SC) at a relatively low peak power of pump pulses ($\sim 10^4$ W). Such a power level is provided by many mode-locked lasers (Ti : sapphire, Cr : forsterite, etc.) without the use of amplification stages.

A relative simplicity of the SC generation by means of special optical fibres and low-power femtosecond lasers stimulated wide applications of SC generators in metrology, tomography, laser spectroscopy, and other fields. The application of holey fibres for SC generation under the action of a continuous train of femtosecond pulsed from a Ti : sapphire laser was experimentally demonstrated for the first time in [13]. In [11], the SC generation from the UV to near-IR range was demonstrated upon propagation of a

S.N. Bagayev, V.I. Denisov, V.F. Zakhar'yash, V.M. Klement'ev, I.I. Korel', S.A. Kuznetsov, V.S. Pivtsov Institute of Laser Physics, Siberian Branch, Russian Academy of Sciences, prosp. Akad. Lavrent'eva 13/3, 630090 Novosibirsk, Russia;
e-mail: clock@laser.nsc.ru;
S.M. Kobtsev, S.V. Kukarin, S.V. Smirnov, N.V. Fateev Novosibirsk State University, ul. Pirogova 2, 630090 Novosibirsk, Russia

Received 17 June 2004
Kvantovaya Elektronika **34** (12) 1107 – 1115 (2004)
Translated by M.N. Sapozhnikov

continuous train of femtosecond pulses from a Ti : sapphire laser in a tapered fibre. Therefore, a highly stable frequency ruler was created, covering the frequency range up to a few terahertz with a step of 0.1 – 1 GHz. This ruler covers broad frequency ranges in the systems for frequency synthesis and substantially simplifies their structure [14, 15]. However, there exist a number of factors restricting the use of such SC generators. These are the amplitude instability of the SC generation, the presence of dips in SC spectra observed upon femtosecond excitation of fibres, a complex temporal structure of emission, etc. The advantages of tapered fibres over holey fibres are that they are cheap and their parameters can be varied in a broad range. Therefore, we report in this paper the study of the emission spectrum of a femtosecond Ti : sapphire laser broadened in a tapered optical fibre.

While the amplitude and spectral parameters of a SC can be comparatively easily investigated with the help of standard instruments, the analysis of the temporal SC structure requires the development of special methods. It seems that for this reason the studies of the temporal SC structure and mechanisms of its formation are at the initial stage at present. Only several papers [16 – 21] were devoted to the experimental and theoretical studies of the temporal distribution of the SC intensity. In this paper, we present the first experimental results of the study of the temporal SC structure in a tapered optical fibre obtained by using the sum frequency generation and give their theoretical interpretation.

2. Broadening of the spectrum of femtosecond pulses in tapered optical fibres

Tapered fibres consist of the input and output parts, conic intermediate regions, and a tapered central part; the fibre cladding and cored diameters decreasing proportionally during fibre drawing. It is in a narrow central region (waist) of the fibre that the spectral broadening of femtosecond pulses occurs. We will show below that the value of this broadening is mainly determined by the ratio of the nonlinear length to the effective length of the fibre and by the dispersion profile of the refractive index of the fibre in the region of the central frequency of laser radiation. The nonlinear length depends on the incident radiation intensity and the effective nonlinear area related to the fibre parameters. The dispersion profile can be found with the help of the characteristic equation for the fundamental mode [22] and the Sellmeyer equation [23].

For the wavelengths of a Ti : sapphire laser in the region from 750 to 850 nm, we can select the fibre waist diameter so that the laser line would lie in the regions of normal, anomalous or zero group-velocity dispersion. Because the process of waist formation can be rather simply controlled, the required diameter and length of the fibre can be easily obtained. This allows the variation of the fibre parameters, by selecting them according to the pump, affecting thereby the shape of the broadened spectrum. The geometry of a tapered fibre itself provides a relative simplicity of a numerical model describing the propagation of pulses and, hence, the formation and broadening of their spectrum.

The main factor determining the spectral broadening of ultrashort pulses in fibres is self-phase modulation (SPM). This nonlinear effect is related to the nonlinear phase shift [24]

$$\psi_{\mathrm{NL}}(z,T) = |U(0,T)|^2 \frac{z}{L_{\mathrm{NL}}}, \tag{1}$$

where L_{NL} is the nonlinear length; z is the waist length; and $U(0,T)$ is the initial pulse shape. The dependence of the nonlinear phase on the pulse shape means that the time derivatives of the phase can be considered as the detuning of the instant frequency from the central frequency at the given point of the pulse. It follows directly from (1) that the broadening of the spectrum will increase with increasing the fibre (waist) length and decreasing its diameter. In addition, we can expect that the broadening will increase with increasing peak power of pulses and decreasing their duration, because in the first case the nonlinear length increases, while in the second – the spectral width of the input pulse. Note that tapered fibres made of multimode fibres are often used in experiments. In this case, the envelope of the output emission spectrum strongly depends on the angle of radiation coupling. Therefore, when optimising the experimental conditions for stabilisation of a femtosecond comb (for example, by means of a stable radio-frequency oscillator), it is very important to estimate theoretically the spectrum envelope at the fibre output, taking all the factors into account. Figure 1 shows the emission spectrum envelopes for two coupling angles.

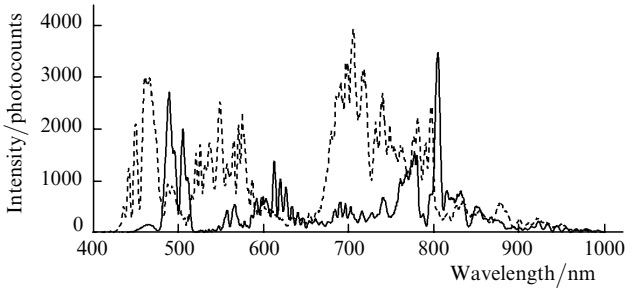

Figure 1. Envelopes of the emission spectrum at the output from a multimode fibre for two angles of radiation coupling to the fibre.

In the general form, the spectrum of a train of ultrashort pulses propagated through a fibre can be represented as a product of the discrete spectrum $F_{\mathrm{d}}(\omega)$, which is typical of spectra for periodic processes, and the envelope $F_{\mathrm{p}}(\omega)$ of an individual pulse in the absence of fluctuations in the train:

$$S(\omega) = F_{\mathrm{p}}(\omega) F_{\mathrm{d}}(\omega). \tag{2}$$

This is a general expression for the spectrum of a train of equal pulses, where $F_{\mathrm{p}}(\omega)$ exactly coincides with the spectrum of one pulse. Note here that this approach assumes the equality of all the parameters of pulses (shape, amplitude, and phase) and also equal time intervals between adjacent pulses in the train.

The statistical analysis of the spectra of pulsed processes is well studied [25, 26]. For example, the phase or amplitude fluctuations of the input train can lead to considerable differences in the shapes and parameters of pulses at the fibre output, so that they can no longer be adequately described by the available statistical models. Experimental spectra can exhibit numerous peaks characteristic of SPM [12], which are caused by the interference between the point of the pulse equally detuned from the central frequency ν_0

[27]. Depending on the phase value at these points and their position in the pulse, the corresponding spectral component can be at the maximum or minimum. Because the nonlinear phase caused by SPM linearly depends on intensity, by coupling to a fibre a train of spectrally broadened pulses with high amplitude fluctuations, we can expect that phase relations for output pulses will be uncertain, resulting in the inevitable distortion of the spectral envelope (Fig. 2). The decrease in the calculated integrated power of the spectral envelope with increasing fluctuation amplitude is explained by the noise enhancement. In fact, the model of the SPM broadening of a train of pulses with unstable amplitudes assumes that the amplitude noise in the fibre is transformed to the phase noise [28].

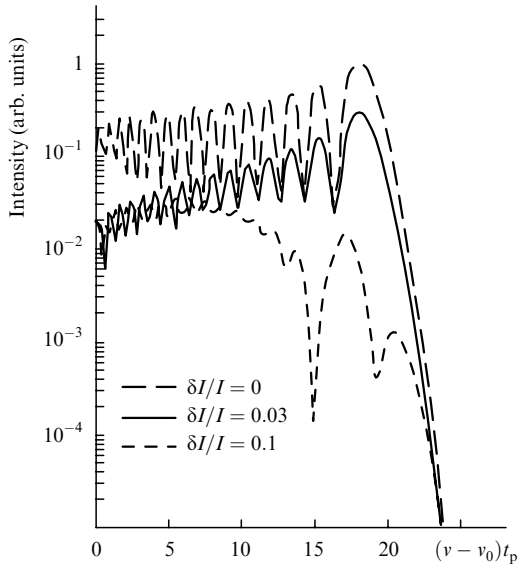

Figure 2. Spectra calculated for trains of 10^2 pulses broadened due to self-phase modulation. The pulses have a Gaussian shape; the pulse duration is $t_p = 30$ fs; the ratio of the waist length to the nonlinear length is $z/L_{NL} = 10^2$. Intensity fluctuations at the fibre input are uniformly distributed in the indicated intervals δI. Because the spectra are symmetric, only positive frequencies $\nu > \nu_0$ are presented.

The theoretical study of formation of the spectral envelope of a train of femtosecond pulses and the numerical solution of the nonlinear Schrödinger equation (NSE) [24] was performed as in [29]. By using the numerical model, we took into account the effect of the group-velocity dispersion (GVD), SPM, the shock wave of the spectral envelope, and SRS on the formation of the emission spectrum of femtosecond lasers propagated through a tapered fibre. Note that to find accurately the spectral profiles of femtosecond pulses, it was necessary to take into account all nonlinear effects, including the development of the shock wave and SRS [30] with dispersion effects of the second and higher orders. The consideration of the high-order dispersion is necessitated by some properties of the propagation of ultrashort pulses in fibres [12, 31, 32] and by the fact that the central wavelength in many experiments is located near the GVD zero, the short-and long-wavelength components of the pulse propagating in the normal and anomalous dispersion regimes, respectively. In the region of anomalous GVD at low powers, when the dispersion length is comparable with the nonlinear length, the soliton regime of SC generation is possible [20, 33]. In the case of normal GVD, the spectrum is broadened mainly due to SPM. Other nonlinear (Raman self-scattering [30], wave-front steeping [34]) and dispersion effects are involved in the spectral-envelope formation, but they do not determine, as a rule, the value of spectral broadening.

Figure 3 shows the calculated and experimental spectra. The comparison of the spectra shows that their broadening is determined by the peak power. This suggests that the broadening of spectra of ultrashort pulses (SC generation) in tapered fibres is caused first of all by SPM, i.e., by the nonlinear phase shift, which is proportional to power. The SPM contribution, as mentioned above, is determined by the ratio z/L_{NL}, while the value of L_{NL} depends on the fibre parameters and radiation power.

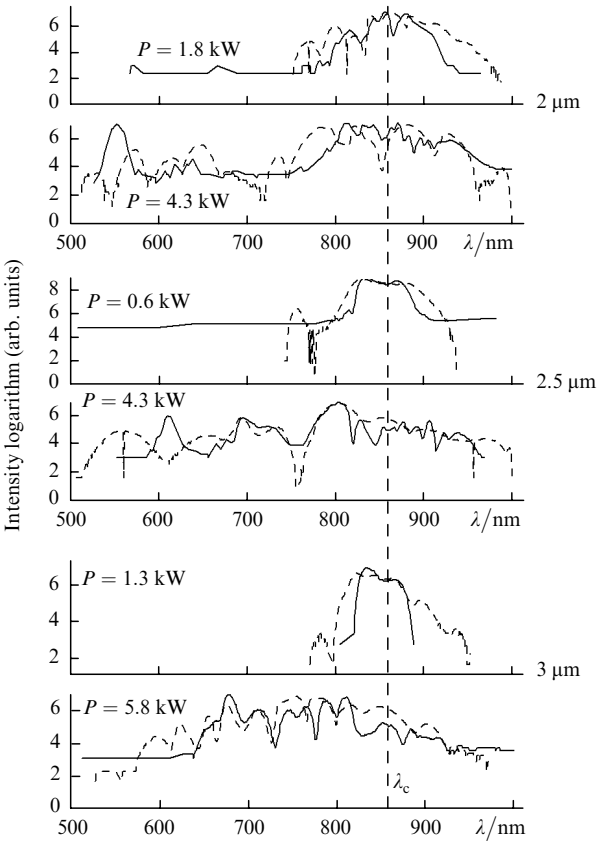

Figure 3. Comparison of the experimental (solid curves) and calculated (dashed curves) envelopes of the spectrum at the fibre output for waist diameters 2, 2.5, and 3 μm and different peak powers of coupled radiation; λ_c is the central wavelength of coupled radiation.

The nonlinear length L_{NL} in our experiments was 6×10^{-2} cm, so that the ratio z/L_{NL} was 10^2. Roughly, this ratio can be treated as the coefficient of spectral broadening caused by SPM. The dispersion length L_D is 20–30 cm, which substantially exceeds both the nonlinear length and the waist size. This means that, when $L_{NL}/L_D \ll 1$, SPM formally dominates over dispersion effects, and formation of the soliton regime and a considerable dispersion increase in the pulse duration is unlikely. Nevertheless, the numerical study showed that dispersion terms are significant even despite a large dispersion length compared to the waist size.

When only SPM acts (dispersion, SRS, and the shock wave are neglected), the solution of the NSE for symmetric

pulses gives symmetric spectra. The pulse shape is simulated, as a rule, by a Gaussian, super-Gaussian or hyperbolic secant. At the same time, most of the experimental spectra (see, for example, [10, 12, 29]) have asymmetric shapes, which suggests the influence of other nonlinear factors and dispersion on the formation of the spectral envelope in tapered fibres. Therefore, although the spectral broadening is mainly determined by SPM, the detailed description of the envelope requires the consideration of all the above factors. The importance of such a description can be illustrated by the fact that in many cases the detected spectra exhibit many peaks, and to control the signal at a fixed wavelength, it is necessary to know not only the reason for the spectral broadening (SPM or soliton regime) but also mechanisms leading to the formation of peaks and dips.

The spectral asymmetry of femtosecond pulses broadened in a tapered fibre is determined by the influence of a dispersion profile, wave-front steeping, Raman self-scattering and the asymmetric pulse shape.

The influence of the dispersion profile is manifested in the fact that the GVD profile is asymmetric with respect to the central radiation wavelength, so that the GVD proves to be different for the two spectral components with the same detuning from both sides of the central frequency, which causes the distortion of the spectrum. The consideration of the high-order dispersion, especially in the cases when the central wavelength is close to the zero-dispersion point, also leads to the asymmetry of the NSE solution and affects the evolution of the spectrum. In addition, recall that the GVD influence can result, under certain conditions, to the formation of solitons.

The steeping of the rear edge of the pulse (the so-called formation of the envelope shock wave) [34] causes the additional spectral broadening of the 'blue' region of the spectrum. However, a simultaneous increase in the time derivative enhances the role of dispersion effects, resulting, in turn, in the increase in the pulse duration, preventing the spectral broadening.

Stimulated Raman self-scattering (intrapulse SRS) [30] is caused by the fact that the 'blue' components of the spectrum can be considered as the pump for 'red' components in the model of classical SRS. Note here that such a mechanism begins to operate for femtosecond pulses already before the spectral broadening caused by other nonlinearities because the spectral width of the incident pulse (20 THz at the 0.1 level) already exceeds the Raman frequency ($\sim$13 THz for glasses) and its efficiency is caused by a high energy density in the waist.

In a number of cases, the Raman term in the nonlinear part of the NSE can cause the formation of the so-called Raman solitons, which along with the formation of anti-Stokes components were studied in microstructure fibres [35].

3. Study of the temporal profile of SC pulses

We studied the temporal profile of SC pulses in a tapered fibre drawn from a standard SMF-28 Corning fibre by the method described in [12]. The fibre waist had the length 7 cm and diameter 2.1 μm, the length of the intermediate region was 2–2.5 cm, the lengths of the input and output undrawn (cylindrical) parts were 5 and 36 cm, respectively.

Figure 4 shows the scheme of the experimental setup for the study of temporal characteristics of a SC generated in a tapered fibre. A train of 50-fs, 795-nm pulses from a Ti : sapphire laser with a repetition rate of 81 MHz propagated through a Faraday isolator, a two-prism compressor, a microobjective, and the initial, undrawn part of the fibre. The compressor was used to compensate the phase modulation (chirp) of pulses, which appeared during their propagation through optical elements of the scheme. After propagation through the Faraday isolator, the pump radiation was divided into two beams. One of the beams was coupled with the help of the $8^{\times}/0.2$ microobjective to the fibre, where broadband emission was generated, while another beam propagated through the controllable time delay line. The SC beam collimated at the fibre output propagated parallel to the pump beam transmitted through the delay line. Both beams were focused by a spherical mirror with the radius of curvature 250 mm into a 1-mm thick nonlinear BBO crystal. The angle between the beams in the crystal was 2.5°. By rotating the BBO crystal, we recorded the sum-frequency emission spectrum. The crystal was rotated by means of an electromechanical drive, which provided a change in the angular position of the BBO crystal by $\pm 15^{\circ}$ at a frequency of up to 20 Hz. The sum-frequency emission spectrum covered the 400–1600-nm region when the reference radiation wavelength was 795 nm and the BBO crystal was rotated by $\pm 15^{\circ}$. For the SC with the typical width 700–1100 nm at the −20-dB level used in these experiments, the sum-frequency emission spectrum was located between 372 and 461 nm.

The sum-frequency emission spectrum produced upon the interaction of pump radiation with the SC was recorded with a spectrometer. The radiation transmitted through the crystal without frequency conversion was suppressed using a

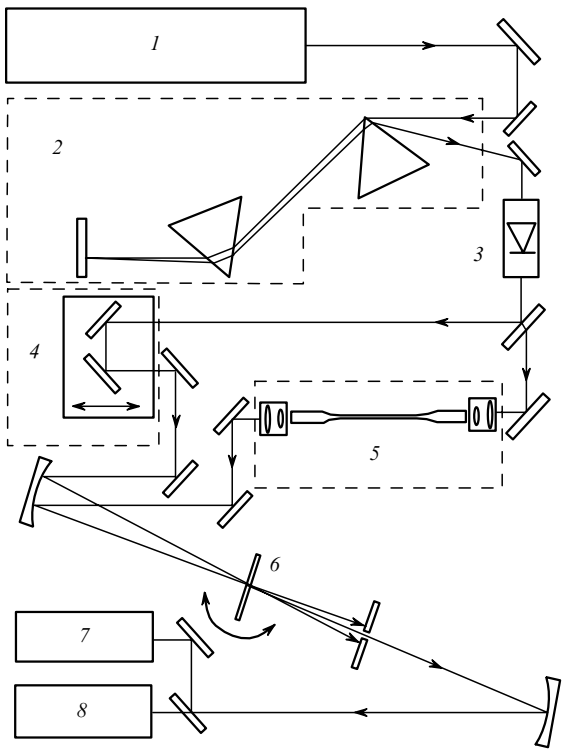

Figure 4. Scheme of the experimental setup: (*1*) femtosecond Ti : sapphire laser; (*2*) two-prism compressor; (*3*) optical isolator; (*4*) delay line; (*5*) tapered fibre; (*6*) nonlinear BBO crystal; (*7*) optical spectrum analyser; (*8*) power meter.

SZS21 filter and a slit shown in Fig. 4. The wavelength of the maximum of the sum-frequency emission spectrum was determined by the delay δt of the reference pulse from the Ti : sapphire laser with respect to the SC pulse. By measuring the delay δt and the wavelength of the maximum of the sum-frequency emission spectrum, we obtained the temporal distribution of the relative intensity $I(\delta t)$ of the SC. The time resolution of $I(\delta t)$ was determined by the reference pulse duration, which increased during the pulse propagation through delay elements and was 125 fs.

Figure 5a shows the emission spectrum generated in the sample under study. The long-wavelength band in the region between 950 and 1050 nm corresponds to the self-shifted soliton [36, 37], while the short-wavelength region corresponds to the pump spectrum broadened due to SPM and SRS. Note that the spectrum presented in Fig. 5a corresponds to the intermediate SC generation regime, so that at a lower pump power a soliton band dominates in the output emission spectrum, while the broadening of the pump spectrum is relatively weak. As the power of pump pulses is increased, they are decomposed into many solitons, resulting in the increase in the efficiency of nonlinear processes and the formation of the broader and smoother SC spectra. The pump power used in our experiments provides, on the one hand, a considerable broadening of the pump spectrum, i.e., the SC generation, and on the other hand, allows us to identify in the output emission spectrum the individual components caused by the self-frequency shift of solitons.

The experimental temporal dependence of the SC intensity (Fig. 5c) exhibits a peak of duration $\sim$1 ps and a long tail extending up to 8 ps.

Figure 6 shows the contour plot of the experimental wavelength distribution of the SC intensity at different instants inside the SC pulse (0–8 ps). The temporal fragments of the SC intensity distribution correspond to the sum-frequency spectra obtained by rotating the BBO crystal at different time delays of the reference pulse from the Ti : sapphire laser. The sum-frequency emission intensity is indicated in Fig. 6 by the shades of grey. The correspondence between the shades of grey in the contour plot and the values of the intensity normalised to unity is shown in the scale at the top right of Fig. 6.

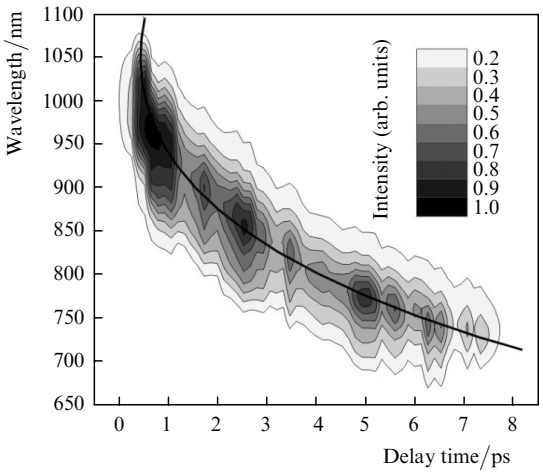

Figure 6. Contour plot $I(\lambda, \delta t)$ and the calculated dependence of the wavelength on the delay time (solid curve).

4. Numerical model

The experimental results were simulated numerically by using the generalised NSE [24]

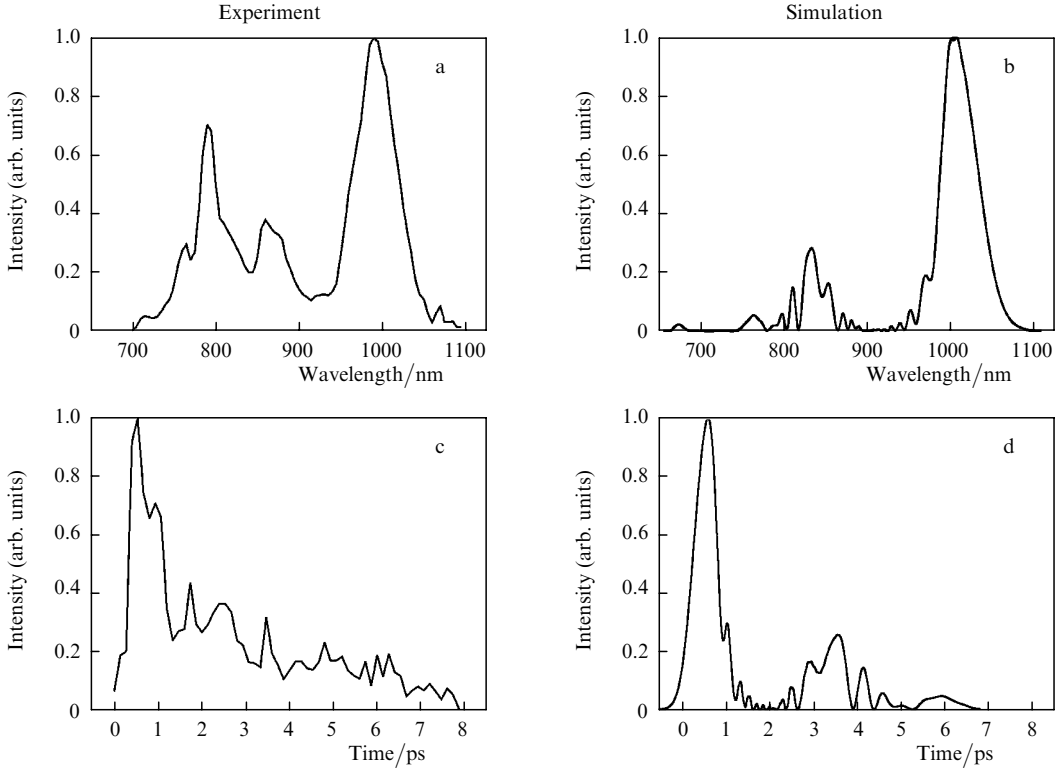

Figure 5. Experimental (a, c) and calculated (b, d) SC intensity distributions over wavelengths and time.

$$\frac{\partial A}{\partial z} = \mathrm{i}\sum_{k=2}^{k_{\max}} \frac{\mathrm{i}^k}{k!}\beta_k \frac{\partial^k A}{\partial t^k} + \mathrm{i}\gamma\left(1 + \frac{\mathrm{i}}{\omega_0}\frac{\partial}{\partial t}\right)$$

$$\times\left[A(z,t)\int_0^\infty R(t')|A(z,t-t')|^2 \mathrm{d}t'\right], \qquad (3)$$

where $A(z,t)$ is the envelope of the electric field strength; β_k is the dispersion coefficients at the pump frequency ω_0; $\gamma = n_2\omega_0/(A_{\mathrm{eff}}c)$ is the nonlinear coefficient; $n_2 = 3.2\times10^{-20}$ m^2 W^{-1} is the nonlinear refractive index of quartz; and A_{eff} is the effective area of the mode base. The kernel $R(t)$ of the integral operator of the nonlinear response of the medium was taken from experiments [38] and it contains both the electronic and vibrational (Raman) contributions.

Equation (3) was obtained without using the slowly-varying amplitude approximation, and can be applied to describe the propagation of few-cycle pulses at the corresponding frequency. It was derived assuming that radiation propagates only in one (fundamental) mode in a fibre. The validity of this assumption is confirmed by the axial symmetry of the intensity distribution at the fibre output. Equation (3) is scalar and it does not describe polarisation effects.

The first term in the right-hand part of (3), the differential time operator, describes the evolution of pulses in the fibre due to dispersion. The term with $k = 2$ describes the increase in the duration of Gaussian pulses caused by linear phase modulation of the pulses during their propagation in the fibre, while the terms with $k > 2$ describe higher-order dispersion effects, which are substantial for femtosecond pulses and also for longer pulses near the zero GVD. In the calculations, we expanded the dispersion operator in a Taylor series in frequency up to the term with $k_{\max} = 5$. The second term in the right-hand term of Eqn (3) describes a number of nonlinear-optical effects such as the self-phase modulation, self-steeping of the envelope wing, formation of shock waves, and SRS [24]. Because of a small (a few tens of centimetres) length of fibres used in experiments, we neglected linear losses in Eqn (3), which cause the exponential decay of the radiation intensity during the propagation of pulses in the fibre. In this case, Eqn (3) does not preserve energy due to SRS, whereas the number of photons is preserved [24, 38].

5. Results and discussion

The results of the numerical simulation are presented in Figs 5b (spectrum) and 5d (the time dependence of the SC). We simulated the propagation of pump pulses through the fibre waist of length 7 cm and diameter 2.1 μm and through the output undrawn part of the fibre of length 36 cm. The propagation of pulses in tapered parts of the fibre with a variable diameter was neglected in the calculations. We also ignored the initial undrawn part of the fibre because phase modulation acquired by the pulse in this part is compensated in the experiment in a two-prism compressor, while nonlinear effects in the undrawn fibre are more than an order of magnitude weaker than those in the fibre waist.

The SC intensity distributions presented in Figs 5a, c qualitatively agree with calculations shown in Figs 5b, d. By comparing the time dependences of the SC intensity, one should bear in mind that the time delay zero is chosen arbitrarily, and only the relative positions of temporal components (peaks) are of importance rather than their absolute time coordinates. Thus, the delay time zero in Fig. 5d was chosen to make the most intense (soliton) peak coincident with the experimental peak in Fig. 5c.

Both the experimental and calculated temporal intensity distributions exhibit the main (soliton) peak at the leading edge of the pulse, which is delayed by 1 ps. The amplitudes of the rest of the peaks decay toward the rear edge of the pulse; however, the number of peaks in the experimental temporal distribution is larger than in the calculated distribution, and they are not resolved, being overlapped. There are no deep intensity dips in the experimental plot, which are observed in the calculated distribution. This can be explained both by a discrete change in the time delay of the reference pulse in the experiment (narrow and deep dips can be unresolved) and by the averaging of experimental pulses over the pump noise. Note also that the calculated pulse is shorter by $\sim$1 ps than the experimental one.

The experimental and calculated SC spectra in Figs 5a, b exhibit the band at 1000 nm with the FWHM of $\sim$50 nm (this band corresponds to an optical soliton, as we will show below). The short-wavelength parts of the spectra are different: the calculated spectrum contains a great number of comparatively narrow bands which are absent in the experimental spectrum. In addition, the intensity dips in the calculated spectrum achieve -30 dB, whereas the intensity between the bands in the experimental spectrum decreases down to the $0.1-0.2$ level. These differences can be explained by the averaging of the spectra over the fluctuations of the pump parameters.

The experimental dependence of the wavelength on the time delay (Fig. 6), can be simply explained as follows. The group velocity near the frequency ω is equal to $1/\beta_1(\omega)$. Therefore, a radiation pulse at the frequency ω propagating over the distance Δz in the fibre waist will change its temporal coordinate by the value

$$\Delta t(\omega) = \beta_1(\omega)\Delta z. \qquad (4)$$

Along with the contour experimental dependence $I(\lambda, \delta t)$, Fig. 6 shows by the thick curve the wavelength dependence of the time delay calculated by (4), taking into account that the pulse propagates a distance of 7 cm in the fibre waist (of diameter 2.1 μm) and a distance of 36 cm in the undrawn fibre. One can see that the calculated wavelength dependence of the time delay well agree with the experiment. This suggests that the relation between the wavelength and temporal coordinate observed in the experiment is caused exclusively by the fibre dispersion (the existence of such a relation was earlier assumed in [16]).

Note that the dependence of the wavelength on the delay time presented in Fig. 6 differs qualitatively from that obtained in [16]: whereas the dependence in Fig. 6 is unique, some values of the time delay in the dependence presented in [16] correspond to two wavelengths. This difference is explained by the fact that in our experiments the dispersion spread of pulsed occurred in the output part of the undrawn fibre (of length 36 cm), whereas the output part of the fibre in [16] was absent. This is illustrated in Fig. 7 showing the dependences of the wavelength on the time delay calculated at eight different points of the output part of the fibre. The longitudinal coordinate of the point, calculated from the beginning of the output part of the fibre, for which the curve is plotted, is presented at each of the curves. Thus, at the

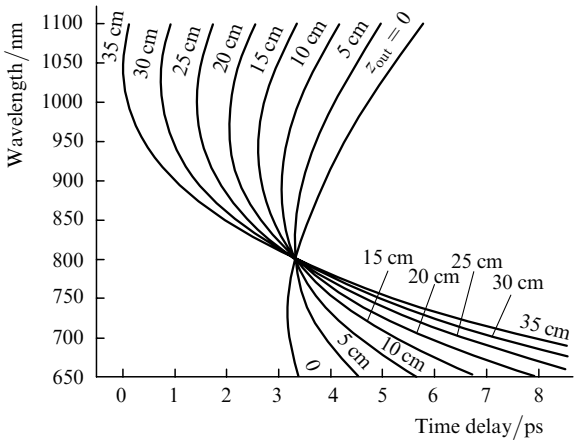

Figure 7. Dependence of the wavelength on the delay time calculated at different points z_{out} of the output part of the fibre.

beginning of the output part ($z_{out} = 0$), the dependence of the wavelength on the delay time presented in Fig. 7 is also ambiguous, i.e., the pulse contains different spectral components at some instances. Then, during the pulse propagation along the output part of the undrawn fibre having the normal GVD (the zero GVD takes place at $\lambda \simeq 1.3$ μm), the long-wavelength components shift to the leading edge of the pulse (their time coordinates decrease), whereas the time coordinates of the short-wavelength components, on the contrary, increase and they shift to the rear edge of the pulse. As a result, after the SC pulse propagated the distance $z_{out} = 35$ cm in the output part of the undrawn fibre, the dependence of the wavelength on the time delay becomes unique virtually over the entire pulse length, as follows from Figs 6 and 7. One should bear in mind that the choice of the time delay zero for each of the dependences in Fig. 7 is arbitrary. We plotted the curves in Fig. 7 so that the time delays at the pump wavelength would be the same.

As mentioned above, the SC investigated in this paper has a comparatively small width (the short-wavelength boundary of the spectrum is located near 700 nm, whereas we obtained earlier [12] in similar fibres the SC extending from 350 to 1140 nm at the −20 dB level) and exhibits a distinct soliton band. The soliton nature of the band is confirmed by its red shift with increasing pump power. In addition, we identified this band as related to solitons by comparing its experimental behaviour with numerical simulations.

To study the propagation dynamics of the calculated pulse in a fibre (which allows us to establish the nature of individual bands in the spectrum and to compare the results with other papers, in particular [16], we consider Fig. 8, which demonstrates twelve plots of the dependence of the calculated intensity on the wavelength and time delay. The plots are calculated for different distances propagated by the pulse in the fibre, which are indicated at the top right angle of each of the plots. The pulse propagates the first 7 cm in the fibre waist of diameter 2.1 μm (the upper row in Fig. 8), and then the SC radiation propagates in the output part of the undrawn fibre (the lower row in Fig. 8). The time delay and wavelength are plotted on the horizontal and vertical axes, respectively, and the shades of grey shows the intensity normalised to unity. The scale of the axes for all the plots is the same.

Analysis of the calculated intensity distributions presented in Fig. 8 allows us to observe the stages of formation of the experimental SC radiation (Fig. 6). Thus, when the pulse propagates a distance of 1 cm in the fibre waist, the width of its spectrum considerably increases, whereas its duration changes weakly (the relative change in the pulse duration at the 0.01 level was 20 % and only 3 % at the 0.1 level). As the radiation further propagates in the fibre waist along the coordinate z ($z = 2 - 7$ cm), its structure changes mainly due to the fibre dispersion. Beginning from $z = 3$ cm, the wavelength dependences of the time delay acquire a quasi-parabolic shape with the extremum at the zero GVD wavelength in the waist (727 nm). During the pulse propagation in the fibre waist, this curve extends along the time axis. The plots for $z = 4 - 7$ cm exhibit two distinct bright spots (with centres at 860 and 1040 nm for $z = 7$ cm), which correspond to optical solitons. The size, shape, and orientation of these spots (peaks in the dependence of the intensity on the wavelength and time) do not change during the pulse propagation along the fibre waist, which is

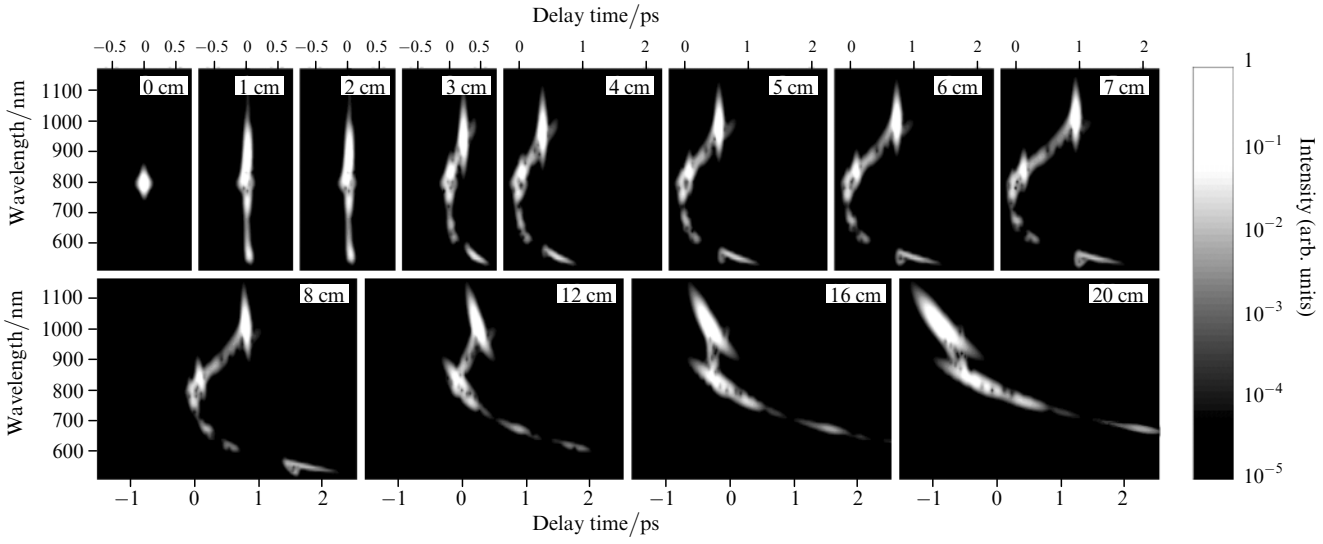

Figure 8. Dependences of the radiation intensity on the wavelength and delay time calculated at different cross sections of the fibre.

explained by the exact mutual compensation of the second-order dispersion and nonlinearity for solitons. Against the background of a strong deformation of the SC spectrum caused by dispersion, one can also see a slow broadening of the spectrum during the SC pulse propagation in the waist (from $z = 1 - 7$ cm), which occurs due to the broadening of both the long-wavelength and short-wavelength wings. A decrease in the carrier frequency of the soliton caused by the higher-order dispersion leads to the broadening of the spectrum to the red, while the short-wavelength components are generated due to the resonance transfer of the soliton energy to this spectral region [33, 39]. Note that the intensity distribution calculated at the output of the fibre waist is in qualitative agreement with the experimental dependence for the SC generated in photonic crystals obtained in [33].

The lower row of plots in Fig. 8 illustrates the evolution of pulses in the first 13 cm of the output part of the undrawn fibre, where the calculated pulse comes after propagation through the waist of length 7 cm. The wavelength of the zero GVD of the undrawn fibre is approximately 1300 nm, so that the entire SC pulse is found in the normal dispersion region, where solitons cannot exist. All the spectral components of the SC propagate in this case with the group velocity of radiation at the corresponding wavelength $v_{gr}(\lambda)$. The group velocity for the long-wavelength components is lower than that for the short-wavelength ones, so that the latter shift to the rear edge of the pulse (their time delays increase), whereas the long-wavelength components shift to the leading edge (their time delays decrease). Because the dependence $v_{gr}(\lambda)$ is monotonic over the entire wavelength range where the SC components exist, the quasi-parabolic dependence of the time delay on the wavelength formed in the fibre waist also becomes monotonic. The initial stage of its evolution is shown in the lower plots in Fig. 8, and the final result – in Fig. 6. Along with the 'straightening' of the entire dependence $\lambda(\delta t)$, we can also see in the plots the deformation of the two bright spots corresponding to solitons in the fibre waist: they expand in time and incline, which suggests the appearance of the phase modulation of the previously soliton pulses, which was absent during the propagation of radiation in the fibre waist.

6. Conclusions

We have presented the results of the study of the emission spectrum of a femtosecond Ti : sapphire laser broadened in a tapered fibre and have found the main properties of the formation of the spectral envelope. The results of our calculations are in qualitative agreement with the experimental data. It is shown that, by varying the fibre parameters and the characteristics of input pulses, the envelope of the broadened spectrum can be shaped, which is important in the use of a femtosecond comb for precision measurements. We have studied the influence of a tapered fibre on the stability of the spectral components of c continuous train of femtosecond pulses from a Ti : sapphire laser. It is shown that a tapered fibre efficiently affects the frequency characteristics of the spectral components of propagating radiation, which makes it suitable for using in precision systems, for example, femtosecond optical clocks and synthesisers.

We have also studied for the first time the temporal structure of the supercontinuum in a drawn fibre by using sum-frequency generation. The plots of the radiation intensity distribution in time are obtained and the dependence of the radiation intensity on the wavelength and time is calculated, which gives the relation between the temporal structure of the supercontinuum pulse and its spectrum. The results of numerical simulations are in good qualitative agreement with the experimental data.

Acknowledgements. This work was supported by the Russian Foundation for Basic Research (Grant No. 03-02-17114a) and the INTAS (Grant No. 03-51-5288).

References

1. Chebotayev V.P., Goldort V.G., Klementyev V.M., Nikitin M.V., Timchenko B.A., Zakhariash V.F. *Appl. Phys. B*, **29**, 63 (1982).
2. Baklanov Ye.V., Chebotaev V.P. *Appl. Phys.*, **12**, 97 (1977).
3. Eckstein J.N., Ferguson A.I., Hänsch T.W. *Phys. Rev. Lett.*, **40**, 847 (1978).
4. Bagayev S.N., Chebotayev V.P., Klementyev V.M., Pyltsin O.I. *Proc. X Int. Conf. Laser Spectroscopy* (Font-Romeu, France, 1991) p. 91.
5. Brabec T., Krausz F. *Rev. Mod. Phys.*, **72**, 545 (2000).
6. Hall J.L., Ye J. *Opt. Photon. News*, February, 44 (2001).
7. Knight J.C., Birks T.A., Russell P.St.J., Atkin D.M. *Opt. Lett.*, **21**, 1547 (1996).
8. Knight J.C., Broeng J., Birks T.A., Russell P.St.J. *Science*, **282**, 1476 (1998).
9. Russell P.St.J. *Laser Focus World*, September, 77 (2002).
10. Zheltikov A.M. *Usp. Fiz. Nauk*, **170**, 1203 (2000).
11. Birks T.A., Wadsworth W.J., Russell P.St.J. *Opt. Lett.*, **25**, 1415 (2000).
12. Kobtsev S.M., Kukarin SV., Fateev N.V. *Kvantovaya Elektron.*, **32**, 11 (2002) [*Quantum Electron.*, **32**, 11 (2002)].
13. Ranka J.K., Windeler R.S., Stentz A.J. *Opt. Lett.*, **25**, 25 (2000).
14. Diddams S.A., Jones D.J., Ye J., Cundiff S.T., Hall J.L., Ranka J.K., Windeler R.S., Holzwarth R., Udem T., Hänsch T.W. *Phys. Rev. Lett.*, **84**, 5102 (2000).
15. Jones D.J., Diddams S.A., Ranka J.K., Stentz A., Windeler R.S., Hall J.L., Cundi S.T. *Science*, **288**, 635 (2000).
16. Dudley M.J., Gu X., Xu L., Kimmel M., Zeek E., O'Shea P., Trebino R., Coen S., Windeler R.S. *Opt. Express*, **10**, 1215 (2002).
17. Xu L., Gu X., Kimmel M., O'Shea P., Trebino R., Galvanauskas A. *CLEO-2001* (Washington, DC: Opt. Soc. Am., 2001) paper CTuN1.
18. Gu X., Xu L., Kimmel M., Zeek E., O'Shea P., Shreenath A.P., Trebino R., Windeler R.S. *Opt. Lett.*, **27**, 1174 (2002).
19. Kobtsev S.M., Smirnov S.V. *Proc. SPIE Int. Soc. Opt. Eng.*, **5480**, 64 (2004).
20. Teipel J., Franke K., Turke D., Warken F., Meiser D., Leuschner M., Giessen H. *Appl. Phys. B*, **77**, 245 (2003).
21. Cao Q., Gu X., Zeek E., Kimmel M., Trebino R., Dudley J., Windeler R.S. *Appl. Phys. B*, **77**, 239 (2003).
22. Snyder A., Love J. *Optical Waveguide Theory* (London, New York: Chapman and Hall, 1983; Moscow: Radio i Svyaz', 1987).
23. Marcuse D. *Light Transmission Optics* (New York: van Nostrand Reinhold, 1982) p. 12.
24. Agrawal G.P. *Nonlinear Fiber Optics* (San Fransisco: Academic Press, 2001).
25. Eliyahu D., Salvatore R.A., Yariv A. *J. Opt. Soc. Am. B*, **13**, 7 (1996).
26. Fuss I.G. *IEEE J. Quantum Electron.*, **30**, 2707 (1994).
27. Shimizu F. *Phys. Rev. Lett.*, **19**, 1097 (1967).
28. Fortier T.M., Ye J., Cundiff S.T., Windeler R.S. *Opt. Lett.*, **27**, 445 (2002).
29. Bagaev S.N., Denisov V.I., Zakhar'yash V.F., Klement'ev V.M., Korel' I.I., Kuznetsov S.A., Pivtsov V.S., Chepurov S.V.

Kvantovaya Elektron., **33**, 883 (2003) [*Quantum Electron.*, 33, 883 (2003)].
30. Dianov E.M. et al. *Pis'ma Zh. Eksp. Teor. Fiz.*, **41**, 242 (1985).
31. Bagayev S.N., Dmitriyev A.K., Chepurov S.V., Dychkov A.S., Klementyev V.M., Kolker D.B., Kuznetsov S.A., Matyugin Yu.A., Okhapkin M.V., Pivtsov V.S., Skvortsov M.N., Zakharyash V.F., Birks T.A., Wadsworth W.J., Russell P.St.J., Zheltikov A.M. *Laser Phys.*, **11**, 1270 (2001).
32. Dianov E.M., Kryukov P.G. *Kvantovaya Elektron.*, 31, 877 (2001) [*Quantum Electron.*, **31**, 877 (2001)].
33. Herrmann J., Griebner U., Zhavoronkov N., et al. *Phys. Rev. Lett.*, **88**, 173 (2002).
34. Tzoar N., Jain M. *Phys. Rev. A*, **23**, 1266 (1981).
35. Washburn B.R., Ralph S.E., Windeler R.S. *Opt. Express*, **10**, 575 (2002).
36. Mitshke F.M., Mollenauer L.F. *Opt. Lett.*, **11**, 659 (1986).
37. Kobtsev S.M., Kukarin S.V., Fateev N.V., Smirnov S.V. *Laser Phys.*, **14**, 748 (2004).
38. Blow K.J., Wood D. *IEEE J. Quantum Electron.*, **25**, 2665 (1989).
39. Husakou A.V., Herrmann J. *Phys. Rev. Lett.*, **87**, 203 (2001).